Analysis of Creep Crack Growth in Surface Cracked Specimens: Comparisons between Approaches of Fracture Mechanics and Continuum Damage Mechanics

Jian-Feng Wen, Shan-Tung Tu*

Key Laboratory of Pressure Systems and Safety (Ministry of Education), School of Mechanical and Power Engineering, East China University of Science and Technology, Shanghai 200237, PR China

*Corresponding author: sttu@ecust.edu.cn

Abstract The numerical approaches to simulate creep crack growth can be divided into two different categories. The first category is employing conventional fracture mechanics, in which the rate of crack growth is predicted by correlating it with a fracture mechanics parameter. The second category gaining much attention is on the basis of damage mechanics concept. In this paper, three dimensional analyses of creep crack growth are performed for 316 stainless steel specimens subjected to tension at high temperature with a semi-elliptical surface crack. Using two independent finite element analyses based on the fracture mechanics and continuum damage mechanics respectively, crack growth behaviors including crack profile development, crack size and propagation time are investigated and compared with each other and corresponding experimental data. The comparisons enable to show the different capabilities of the two approaches in predictions of creep crack growth.

Keywords Creep crack growth, Fracture mechanics, Continuum damage mechanics, Finite element analysis

1. Introduction

The increased computational power and programming capabilities have given impetus to the numerical prognoses of the structural integrity and service-ability throughout the lifetime of structures at high temperature. During the past decades, the numerical approaches to simulate creep crack growth have developed into two different groups. The first group is employing conventional fracture mechanics, in which the crack growth rate is predicted by correlating it with a fracture mechanics parameter such as stress intensity factor or C^*-integral [1-4]. The second group is based on damage mechanics concept [5]. When the creep damage variable reaches a critical value, material failure is considered to occur, and thus crack growth can be characterized by a completely damaged element zone ahead of the initial crack tip [6-9]. Alternatively, a node-release technique has been employed to simulate the separation of the crack face [10-14]. However, little research has been successfully conducted in applying the two approaches to three dimensional analysis of creep crack propagation. Furthermore, there is a need for a better understanding of the different capabilities of the two approaches in predictions of crack growth under creep conditions.

In this paper, three dimensional analyses of creep crack growth are performed for 316 stainless steel specimens subjected to tension at high temperature with a semi-elliptical surface crack. Section 2 briefly describes the conventional fracture mechanics models and a damage-based model recently proposed by the authors. The main idea of the two approaches in conjunction with the finite element (FE) method is demonstrated in Section 3. Subsequently, Section 4 shows the comparisons of

predictions using two independent analyses based on the two methods respectively. The conclusions are made in Section 5.

2. Mechanical model

2.1 Geometrical description

Thumbnail crack specimens tested at 600ºC by Hyde [15] subjected to static loads of tension are considered in the study, as shown in Fig. 1. The crack region can be divided into three parts: initial notch, fatigue crack and creep crack. In this work, attention is mainly paid to the creep crack region. Two specimens with extensive creep crack growth are chosen, of which test conditions are summarized in Table 1.

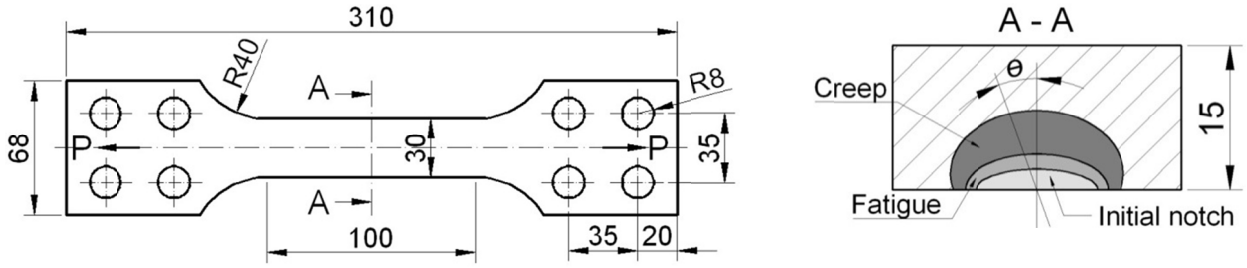

(a) (b)

Figure 1. Geometry of a thumbnail crack specimen: (a) a whole geometry; (b) an enlarged section view on A-A.

Table 1. Test conditions for the thumbnail crack specimens tested at 600 ºC.

Specimen No.	Initial creep crack size (mm)		Load (N)	Test duration (h)
	at $\theta = 0º$	at $\theta = 90º$		
5	2.88	4.33	90800	2760
6	3.50	4.37	90700	1200

2.2 Elasticity-secondary creep and creep fracture parameter

Basically, the time-dependent deformation characteristics for 316 stainless steel can be described by the following classical elastic-secondary creep constitutive relation

$$\dot{\varepsilon} = \frac{\dot{\sigma}}{E} + A\sigma^n, \tag{1}$$

where $\dot{\varepsilon}$ and $\dot{\sigma}$ denote the derivative of strain and stress corresponding to time; E is the Young's modulus; A and n are steady-state creep coefficient and steady-state creep exponent respectively. The material constants employed in FE analysis are listed in Table 2 [1, 9, 15].

For structures operated under creep regime, C^* is a proper fracture mechanics parameter to describe the crack growth. With regard to actual components such as plates and pipes, the values of C^* need to be determined by using FE methods. Then, with the transition time from small scale creep to the steady state ignored, the crack growth rate is represented in the following form:

$$\frac{da}{d\tau} = C(C^*)^q, \tag{2}$$

where τ, C and q denote the time, creep crack growth coefficient and exponent, respectively. Provided C^* has the unit of $Nmm^{-1}h^{-1}$, C and q for tests of compact tension (CT) specimens of 316 stainless steel at 600ºC [15] are also shown in Table 2.

Table 2. Material properties of the 316 stainless steel tested at 600ºC.

E (MPa)	ν	A ($MPa^{-n}h^{-1}$)	n	C	q	ε_f (%)
148000	0.3	1.47×10^{-29}	10.147	2.774×10^{-2}	0.958	27

2.3 Creep-damage model

The continuum damage mechanics model can trace its roots to Kachanov and Rabotnov's work [16, 17]. Since then there have been many attempts to develop an appropriate model [5, 18-20]. Recently, the authors presented a creep-damage model to simulate creep fracture, which is capable of characterizing the full creep curve and can reasonably reflect the influence of stress state on creep deformation and damage. More detailed description and validation of the proposed creep-damage model can be found in Refs. [21, 22]. The proposed model is as follows:

$$\dot{\varepsilon}_{ij}^c = \frac{3}{2} A\sigma_e^{n-1} s_{ij}\left[1+\beta\left(\frac{\sigma_1}{\sigma_e}\right)^2\right]^{\frac{n+1}{2}}, \tag{3}$$

and

$$\dot{\omega} = \frac{\dot{\varepsilon}^c}{\varepsilon_f^*}, \tag{4}$$

where A and n are material constants. ε_{ij}^c, s_{ij}, σ_e and σ_1 are the creep strain tensor, deviatoric stress tensor, equivalent stress and maximum principle stress, respectively. ω, $\dot{\varepsilon}^c$ and ε_f^* denote the damage variable, creep strain rate and multi-axial creep failure strain, respectively. β is a stress-independent function reflecting material behavior, having the form

$$\beta = \frac{2\rho}{n+1} + \frac{(2n+3)\rho^2}{n(n+1)^2} + \frac{(n+3)\rho^3}{9n(n+1)^3} + \frac{(n+3)\rho^4}{108n(n+1)^4}, \tag{5}$$

where the micro-crack damage parameter, ρ, depends primarily on the number of micro-cracks per unit volume and their average diameter. Suppose the damage variable is given as the reduction of the effective area in the cell, we can obtain

$$\rho = \frac{2(n+1)}{\pi\sqrt{1+3/n}}\omega^{3/2}. \tag{6}$$

It is known that the creep ductility significantly depends on the stress state. In this work, a modified multi-axial ductility model, which can describes the behavior of creep cavity growth more appropriately than the widely-used Cocks-Ashby model [23], is employed:

$$\frac{\varepsilon_f^*}{\varepsilon_f} = \exp\left[\frac{2}{3}\left(\frac{n-0.5}{n+0.5}\right)\right] \Big/ \exp\left[2\left(\frac{n-0.5}{n+0.5}\right)\frac{\sigma_m}{\sigma_e}\right], \tag{7}$$

where ε_f is the uniaxial creep failure strain and σ_m is the hydrostatic stress. In this work, the optimum value of ε_f for tests of uniaxial specimens of 316 stainless steel at 600ºC is found to be 0.27, as listed in Table 2.

3. Finite element framework

3.1 Using fracture mechanics approach

To predict the crack growth behavior of thumbnail crack specimens under creep conditions, fracture mechanics approach has been used in conjunction with the FE method. Numerical simulations of creep crack growth, which have been based on a step-by-step analysis procedure, are described as follows:

(a) Creating of the FE models. One quarter of the specimen containing a semi-elliptical surface crack has been created using the codes ABAQUS [24] and ZENCRACK [25] due to symmetry of both the geometry and loading. About 10,000 elements of type C3D8I for each model have been adopted. Note that extremely refined meshes are generated in the crack tip zone to obtain accurate results.

(b) Calculations of values of C^*. Values of C^* at a set of points which constitute the crack front can be calculated using the equivalent domain integral (EDI) method provided by the codes ABAQUS. In the study, the crack front has been divided into 16 sections, so values of C^* at 17 points are recorded in every step.

(c) Calculation of the increment of the crack size. The steady-state creep crack growth can be represented by Eq. (2), according to which, the creep crack growth increment at each point along the crack front, Δa_i, can be calculated as

$$\Delta a_i = \left(\frac{C_i^*}{C_{\max}^*}\right)^q \Delta a_{\max}, \tag{8}$$

where C_i^* and $C_{\max}^*$ are C^* at an arbitrary point and the maximum value along the crack front, respectively; $\Delta a_{\max}$ denote the maximum crack growth increment at the point where $C_{\max}^*$ occurs.

(d) Establishment of a new crack profile. Based on the creep crack increment at each point along the crack front, a set of new points can be determined. And then, a new crack profile can be created by using codes ZENCRACK.
(e) Returning to stage (a). The crack continued to extend through the stages from (a) to (d) until a termination condition is reached.

3.2 Using continuum damage mechanics approach

Creep damage modeling has been also carried out using the codes ABAQUS with the elastic-plastic-creep properties of 316 stainless steel tested at 600ºC [1, 9, 15]. The total strain can be calculated by

$$\varepsilon^{tol} = \varepsilon^{e} + \varepsilon^{p} + \varepsilon^{c}, \tag{9}$$

where $\varepsilon^{e}, \varepsilon^{p}$ and ε^{c} are elastic, plastic and creep strain components, respectively. The true stress-strain data beyond the yield point is used as input to FE analysis and a Mises flow rule with isotropic strain hardening is employed. To define the time-dependent and damage-coupled creep behavior, Eq. (3) is implemented into the ABAQUS user subroutine, CREEP. Eq. (4) is also embedded in CREEP to determine the damage accumulation. Creep damage variable, ω, is in the range of 0 to 0.99. When ω at a Gauss point reaches 0.99, all the stress components are sharply reduced to a small plateau and thus crack growth can be characterized by a completely damaged element zone ahead of the initial crack tip. Another user subroutine, USDFLD, is employed to embody this failure simulation technique.

Using this numerical method, three-dimensional creep damage analyses are performed to simulate the creep crack growth in thumbnail crack specimens. One quarter of the model consisting of about 10,000 eight-node C3D8R elements is modeled exploiting the symmetry conditions. The mesh size in the vicinity of the crack front is 200μm, which has been proved to provide excellent predictions in Ref. [21].

4. Results and discussion

4.1 Predictions using fracture mechanics approach

To achieve accurate predictions of crack growth using fracture mechanics approach, it is essential to choose a proper maximum crack growth increment, $\Delta a_{\max}$, in Eq. (8). Comparison of crack depth variations predicted using five different maximum crack growth increments, $\Delta a_{\max} = t/300$, $t/150$, $t/75$, $t/30$ and $t/15$, for the thumbnail crack in specimen 5 is shown in Fig. 2. It can be seen that the difference between the crack depth variations cannot be neglected when the maximum crack growth increment is relatively large ($\Delta a_{\max} = t/30$ and $t/15$). For $\Delta a_{\max} = t/300$, $t/150$ and $t/75$, however,

difference between predictions is extraordinarily hard to identify on the plot, which demonstrates the convergence of the relation between the crack depth and propagation time does exist. In this paper, the maximum crack growth increment is selected as $t/150$, which is small enough to achieve a required accuracy of crack growth time.

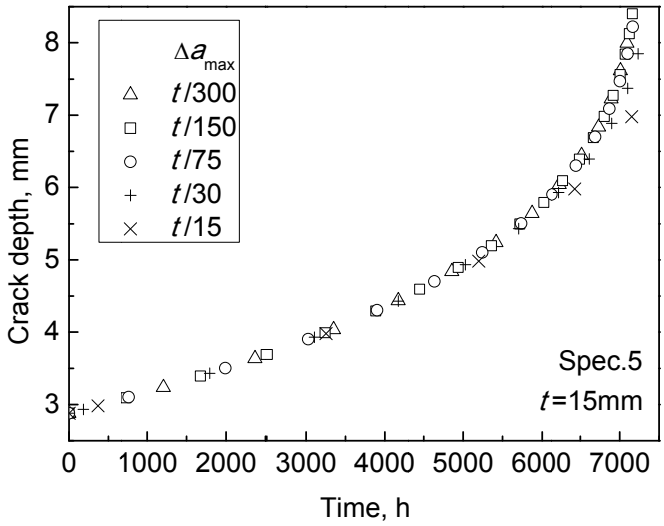

Figure 2. Comparison of crack depth variations predicted using five different maximum crack growth increments

Fig. 3 shows the predicted creep crack shape developments for thumbnail cracks in specimens 5 and 6 with the initial semi-elliptical crack front. It can be found that the increment along depth direction is always more considerable than that along surface direction at each step. As a result, the accumulative increment of crack depth is obviously larger than that of half crack length.

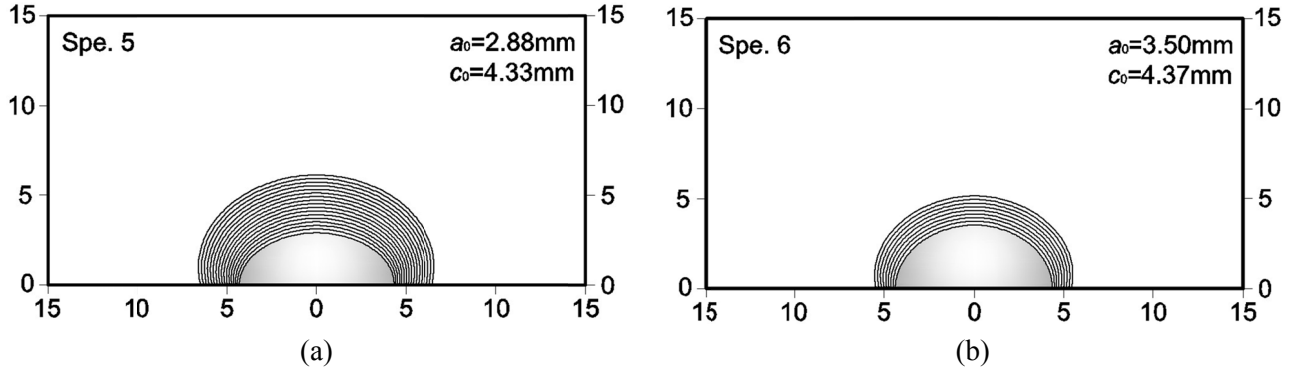

Figure 3. Predicted creep crack shape evolutions resulting from fracture mechanics approach: (a) specimen 5; (b) specimen 6

Fig. 4 depicts the tested specimen photos taken from Ref [9, 15] and predictions using fracture mechanics approach for specimens 5 and 6. It can be said that the predicted crack fronts are similar to the experimental results for both specimens. Nevertheless, the predicted propagations times are 2~3 times as long as the actual test durations. This is mainly because that creep crack growth coefficient and exponent, C and q, in Eq. (2) are obtained from the correlation of da/dt and C^* for tests of CT specimens instead of the investigated thumbnail crack specimens. For a given C^*, the

crack growth rate for a crack in a CT specimen can be considerably lower than in a thumbnail crack specimen due to the different constraint effect of varied types of specimens.

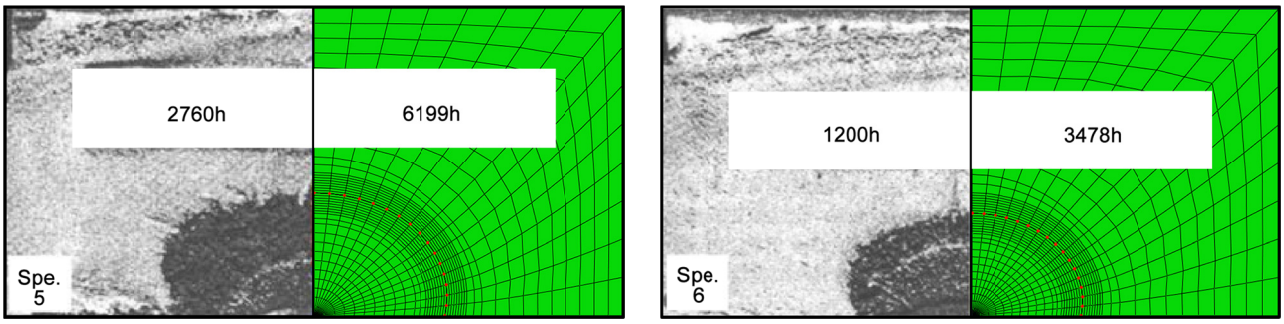

(a) (b)

Figure 4. Comparisons of tested specimen photos with predictions using fracture mechanics approach: (a) specimen 5; (b) specimen 6

4.2 Predictions using continuum damage mechanics approach

Predicted crack profiles using continuum damage mechanics approach are compared with the tested specimen photos in Fig. 5. Obviously, the FE predicted crack fronts match very closely to the experimental results. One can also find that the crack propagates with larger increment at $\theta = 0^{\circ}$ (approximately under plane-strain condition) than that at $\theta = 90^{\circ}$ (approximately under plane-stress condition) due to the constraint effect. Propagation times predicted by the numerical simulation are also in good agreement with the test durations. These encouraging results prove the validity and predictive capability of the proposed creep-damage model presented in Eqs. (3) and (4).

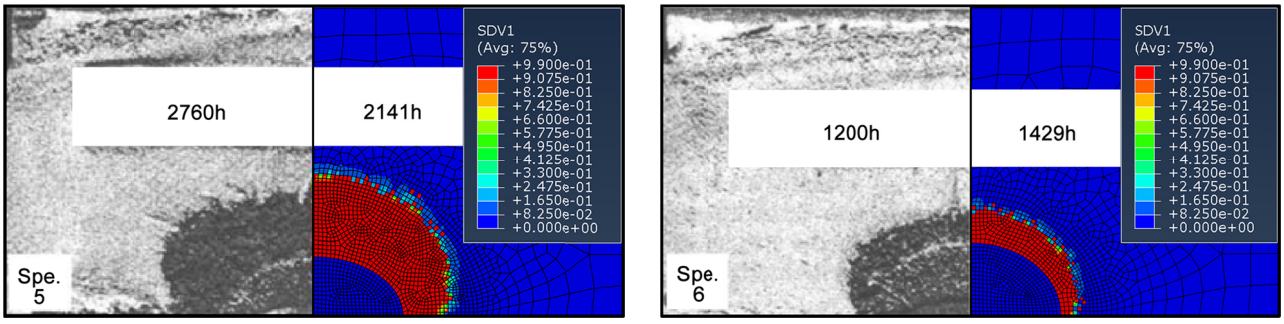

(a) (b)

Figure 5. Comparisons of tested specimen photos with predictions using continuum damage mechanics approach: (a) specimen 5; (b) specimen 6

Fig. 6 provides comparisons of crack depth variations predicted by using fracture mechanics and continuum damage mechanics approaches. It is clear that damage mechanics predictions are more closely to the experimental data. In addition, the crack initiation times, nearly 500 hours, can also be predicted by continuum damage mechanics approach. When C^*-type method is employed, no information regarding crack initiation can be obtained.

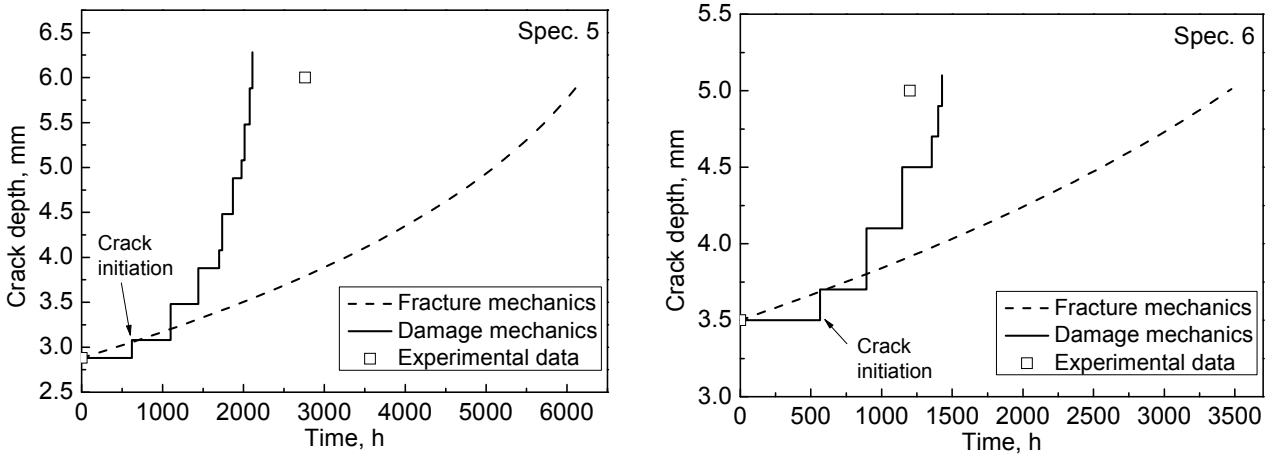

(a) (b)

Figure 6. Comparisons of crack depth variations predicted by using fracture mechanics and continuum damage mechanics approaches

5. Conclusions

The main conclusions drawn from the study are listed as follows:

(a) For fracture mechanics approach, the convergence of the relation between the crack depth and propagation time does exist if the maximum crack growth increment is small enough.

(b) Both fracture mechanics and continuum damage mechanics approaches in conjunction with the FE technique can give reasonable predictions of the crack profile when compared with the experimental results of thumbnail crack specimens tested under tension.

(c) The propagation time can also be appropriately predicted by the damage mechanics approach, while it is far from satisfactory when using the facture mechanics method. For the purpose of a more accurate prediction, the different constraint effects between the CT and thumbnail crack specimen need to be carefully considered.

(d) The crack initiation time can also be predicted by the damage-based approach presented in the study.

Acknowledgements

This work is financially supported by National Natural Science Foundation of China (Contract No. 50835003). The authors would also like to thank Prof. T.H. Hyde and Prof. W. Sun at University of Nottingham for the helpful discussion with them.

References

[1] Smith SD, Webster JJ, Hyde TH. Creep behaviour of a stationary, semicircular surface crack. Engng Fract Mech 1988;30:105-16.

[2] Yoon KB, Park TG, Saxena A. Creep crack growth analysis of elliptic surface cracks in pressure vessels. Int J Pres Ves Pip 2003;80:465-79.

[3] Kayser Y, Marie S, Poussard C, Delaval C. Leak Before Break procedure: Recent modification of RCC-MR A16 appendix and proposed improvements. Int J Pres Ves Pip 2008;85:681-93.
[4] Wen JF, Tu ST, Gong JM, Sun W. Creep fracture mechanics parameters for internal axial surface cracks in pressurized cylinders and creep crack growth analysis. Int J Pres Ves Pip 2011;88:452-64.
[5] Lemaitre J, Desmorat R. Engineering damage mechanics: ductile, creep, fatigue and brittle failures. Berlin: Springer-Verlag; 2005.
[6] Oh CS, Kim NH, Kim YJ, Davies C, Nikbin K, Dean D. Creep failure simulations of 316H at 550 degree C: Part I: method and validation. Engng Fract Mech 2011;78:2966-77.
[7] Oh CS, Kim NH, Min SH, Kim YJ. Finite element damage analysis for predictions of creep crack growth. Proceedings of the ASME 2010 Pressure Vessels & Piping Division / K-PVP Conference. Washington, USA. 2010.
[8] Hyde TH, Saber M, Sun W. Testing and modelling of creep crack growth in compact tension specimens from a P91 weld at 650 degree C. Engng Fract Mech 2010;77:2946-57.
[9] Hyde CJ, Hyde TH, Sun W, Becker AA. Damage mechanics based predictions of creep crack growth in 316 stainless steel. Engng Fract Mech 2010;77:2385-402.
[10] Yatomi M, Tabuchi M. Issues relating to numerical modelling of creep crack growth. Engng Fract Mech 2010;77:3043-52.
[11] Yatomi M, Davies CM, Nikbin KM. Creep crack growth simulations in 316H stainless steel. Engng Fract Mech 2008;75:5140-50.
[12] Yatomi M, O'Dowd NP, Nikbin KM, Webster GA. Theoretical and numerical modelling of creep crack growth in a carbon-manganese steel. Engng Fract Mech 2006;73:1158-75.
[13] Yatomi M, Bettinson AD, O'Dowd NP, Nikbin KM. Modelling of damage development and failure in notched-bar multiaxial creep tests. Fatigue Fract Engng Mater Struct 2004;27:283-95.
[14] Yatomi M, Nikbin KM, O'Dowd NP. Creep crack growth prediction using a damage based approach. Int J Pres Ves Pip 2003;80:573-83.
[15] Hyde TH. Creep crack growth in 316 stainless steel at 600 degree C. High Temp Technol 1988;6:51-61.
[16] Rabotnov YN. Creep problems in structural members. Amsterdam: North-Holland; 1969.
[17] Kachanov LM. Rupture time under creep conditions. Int J Fracture 1999;97:11-8.
[18] Liu Y, Murakami S. Damage localization of conventional creep damage models and proposition of a new model for creep damage analysis. JSME Int J Ser A 1998;41:57-65.
[19] Murakami S, Liu Y. Mesh-dependence in local approach to creep fracture. Int J Damage Mech 1995;4:230.
[20] Murakami S, Liu Y, Mizuno M. Computational methods for creep fracture analysis by damage mechanics. Comput Meth Appl Mech Engng 2000;183:15-33.
[21] Wen JF, Tu ST, Gao XL, Reddy JN. Simulations of creep crack growth in 316 stainless steel using a novel creep-damage model. Engng Fract Mech 2013; doi: http://dx.doi.org/10.1016/j.engfracmech.2012.12.014.
[22] Wen JF, Tu ST, Gao XL, Reddy JN. A new model for creep damage analysis and its application to creep crack growth simulations. 9th International Conference on Creep and Fatigue at Elevated Temperatures. London, UK. 2012.

[23] Cocks AF, Ashby MF. Intergranular fracture during power-law creep under multiaxial stresses. Metal Sci 1980;8:395-402.
[24] ABAQUS. Version 6.9-EF ed. Providence: Dassault Systèmes; 2009.
[25] ZENCRACK. Version 7.7 ed. London: Zentech International Limited; 2012.